LYCEN/8575
Novembre 1985

RPA spin-isospin nuclear response in the deep inelastic region

W. M. Alberico and A. Molinari

Istituto di Fisica Teorica dell'Università di Torino
corso M. d'Azeglio 46 - 10125 Torino (Italy)
and
I. N. F. N., Sezione di Torino, Torino, Italy

A. De Pace

Institut für Theoretische Physik, Universität Tubingen
Auf der Morgenstelle 14 - D7400 Tubingen (W. Germany)
and
I. N. F. N., Sezione di Torino, Torino, Italy

M. Ericson

Institut de Physique Nucléaire (and IN2P3)
Université Claude Bernard Lyon-1, 69622 Villeurbanne Cedex, France

and
CERN, Geneva (Switzerland)

M. B. Johnson

Los Alamos Scientific Laboratories, LAMPF
Los Alamos, NM 87545 (USA)

Abstract

The spin-isospin volume responses of a finite nucleus are evaluated in the RPA frame, utilizing a harmonic oscillator basis. Particular emphasis is given to the mixing between the longitudinal ($\vec{\sigma}\cdot\vec{q}$) and transverse ($\vec{\sigma}\times\vec{q}$) couplings, which arise at the nuclear surface. We show that it reduces somewhat the contrast between the two spin responses. We compare the calculated transverse response with the experimental one extracted from deep inelastic electron scattering.

1. Introduction

The nuclear spin-isospin response has been the subject of active investigations, both experimentally and theoretically. The (e,e') experiments have provided accurate data [1] in the transverse channel for a number of nuclei. These results allow the search for collective effects, expected as a remnant, at finite momentum transfers, of the giant Gamow Teller resonance. In the spin longitudinal channel, on the other hand, collective effects, if they exist, are of particular interest, being precursors of pion condensation.

Up to now most of the theoretical descriptions have relied on nuclear matter evaluations, either directly in infinite [2,3] or semi-infinite [4] systems, or indirectly, as in semiclassical approaches [5]. An exception is the continuum RPA calculation of the spin transverse response in ^{12}C by Cavinato et al. [6].

Experimentally a universal behaviour of the transverse response per particle has been observed in medium nuclei [1], suggesting the volume character of the response, which can thus be reasonably described by a nuclear matter treatment. Nevertheless it is of interest to solve the RPA equations in a finite system in order to elucidate the role of the nuclear surface.

The influence of the latter is twofold: indeed the surface brings down the density felt by the peripheral nucleons thus suppressing some collectivity. This aspect is properly accounted for already in a semiclassical approach [7]. Moreover an additional suppression can arise from the variation in space of the nuclear density, as it was shown to occur in the static situation [8]. These features, which are totally absent in a nuclear matter treatment, have not yet been systematically investigated.

One of the aims of this work is to shed light on their importance; in particular the density gradient arising at the surface introduces a coupling between the $(\vec{\sigma}, \vec{q})$ and the $(\vec{\sigma} \times \vec{q})$ vertices, thus reducing the contrast between the two spin responses.

Such effects are obviously enhanced when only the surface is explored by the probe, as it happens in (p,p') scattering. The surface response will be treated separately in a forthcoming paper [9]; here we will restrict ourselves to the volume responses, as probed in (e,e') scattering.

We will evaluate the two spin responses from the generalized polarization propagators $\Pi_{\mu\nu}(\vec{q},\vec{q}';\omega)$. The RPA equations for these quantities have been written in ref.[10]; here we will solve them in the approximation suggested by Toki and Weise [11] (hereafter referred to as TW), partly to avoid the heavy numeric required by the search for an exact solution and partly because their scheme leads to analytic formulae which transparently display the connection with the infinite nuclear matter response as well as the new features introduced by the surface.

The paper is organized as follows: Section 2 reviews those elements of reference [10] which are needed for the present study. In Section 3 we give the explicit formulae for the spin-isospin responses, based on the TW approximation. We also give some insight on the validity of this approximation by investigating the non-locality in momentum space of $\Pi^0(\vec{q},\vec{q}';\omega)$.

Section 4 contains the results of the present approach utilizing an Harmonic Oscillator (H.O.) basis; they are compared with the ones obtained in a semiclassical approximation [5]. In particular we discuss the validity of the H.O. basis with respect to a more realistic one. Finally we compare our results for the transverse response with the existing experimental data.

2. The spin-isospin nuclear response

In ref.[10] the transverse spin-isospin response is defined as follows

$$R_T(q,\omega) = -\frac{1}{\pi}\sum_{m,n}\delta_{m,n}\,\mathrm{Im}\,\Pi_{m3,n3}(\vec{q},\vec{q};\omega) \qquad (2.1)$$

in terms of the spherical "spatial" components $m,n = 0,\pm1$ of $\Pi_{\mu\nu}(\vec{q},\vec{q}';\omega)$, whereas the longitudinal one

$$R_L(q,\omega) = -\frac{1}{2\pi}\,\mathrm{Im}\,\Pi_{03,03}(\vec{q},\vec{q};\omega) \qquad (2.2)$$

is fixed by the $\mu=\nu=0$ ("time") components. In (2.1) and (2.2) the index 3 denotes isospin.

By a suitable multipole expansion $\Pi_{\mu\nu}(\vec{q},\vec{q}';\omega)$ can be factored out in a geometrical and a dynamical part (see ref.[10] for the explicit formulae). The latter obeys, in the RPA frame, to the following set of integral equations

$$\left[\hat{\Pi}^{RPA}_J(q,q';\omega)\right]_{\ell\ell'} = \left[\hat{\Pi}^{\circ}_J(q,q';\omega)\right]_{\ell\ell'} +$$

$$+\frac{1}{(2\pi)^3}\int_0^\infty dk\,k^2 \sum_{\ell_1\ell_2}\left[\hat{\Pi}^{\circ}_J(q,k;\omega)\right]_{\ell\ell_1}\left[U_J(k)\right]_{\ell_1\ell_2}\left[\hat{\Pi}^{RPA}_J(k,q';\omega)\right]_{\ell_2\ell'} \qquad (2.3)$$

The first term in the RHS is the dynamical factor of the

independent particle polarization propagator: if the spin-orbit term in the mean field is disregarded it turns out to be diagonal in the angular momenta, i.e. $\hat{\Pi}^{\circ}_J(q,q';\omega)_{\ell\ell'} = \delta_{\ell\ell'}\,\hat{\Pi}^{\circ}_\ell(q,q';\omega)$, and reads (the indices "p" and "h" indicate particle and hole, respectively)

$$\hat{\Pi}^{\circ}_\ell(q,q';\omega) = 16\pi\sum_{\substack{n_p\ell_p\\ n_h\ell_h}}(2\ell_p+1)(2\ell_h+1)\begin{pmatrix}\ell_p & \ell_h & \ell\\ 0 & 0 & 0\end{pmatrix}^2 \mathcal{J}_{\ell_{n_p\ell_p n_h\ell_h}}(q)$$

$$\left\{\frac{1}{\hbar\omega-(\epsilon_{n_p\ell_p}-\epsilon_{n_h\ell_h})+i\eta}-\frac{1}{\hbar\omega+(\epsilon_{n_p\ell_p}-\epsilon_{n_h\ell_h})-i\eta}\right\}\mathcal{J}_{\ell_{n_p\ell_p n_h\ell_h}}(q') \qquad (2.4)$$

where

$$\mathcal{J}_{\ell_{n_p\ell_p n_h\ell_h}}(q) = q\int_0^\infty dr\,r^2\,j_\ell(qr)\,R_{n_p\ell_p}(r)\,R_{n_h\ell_h}(r). \qquad (2.5)$$

In the above the $R_{n\ell}(r)$ are the radial wave functions, belonging to the eigenvalues $\epsilon_{n\ell}$. In principle they should be self-consistently calculated. In practice we shall use the eigenfunctions of an harmonic oscillator with the strength fixed by the experimental size of the system. They should at least contain the information on the confinement of the system.

In the following $\hat{\Pi}^{\circ}$ will also include the Δ-h propagator, assuming for the isobar the same mean field as for the nucleons.

Now when the nuclear spin-isospin responses (2.1) and (2.2) are explicitly expressed through the $\hat{\Pi}^{RPA}_J$ components diagonal in momentum space, they turn out to be given by the

following combinations

$$R_T(q,\omega) = -\frac{1}{16\pi^2}\sum_{J=1}^{\infty}\Big\{(J+1)\,\mathrm{Im}\Big[\hat{\Pi}^{RPA}_J(q,\omega)\Big]_{J-1,J-1}$$

$$+\sqrt{J(J+1)}\,\mathrm{Im}\Big\{\Big[\hat{\Pi}^{RPA}_J(q,\omega)\Big]_{J-1,J+1}+\Big[\hat{\Pi}^{RPA}_J(q,\omega)\Big]_{J+1,J-1}\Big\} \qquad (2.6)$$

$$+(2J+1)\,\mathrm{Im}\Big[\hat{\Pi}^{RPA}_J(q,\omega)\Big]_{J,J}+J\,\mathrm{Im}\Big[\hat{\Pi}^{RPA}_J(q,\omega)\Big]_{J+1,J+1}\Big\}$$

and

$$R_L(q,\omega) = -\frac{1}{8\pi^2}\sum_{J=0}^{\infty}\Big\{J\,\mathrm{Im}\Big[\hat{\Pi}^{RPA}_J(q,\omega)\Big]_{J-1,J-1}$$

$$-\sqrt{J(J+1)}\,\mathrm{Im}\Big\{\Big[\hat{\Pi}^{RPA}_J(q,\omega)\Big]_{J-1,J+1}+\Big[\hat{\Pi}^{RPA}_J(q,\omega)\Big]_{J+1,J-1}\Big\} \qquad (2.7)$$

$$+(J+1)\,\mathrm{Im}\Big[\hat{\Pi}^{RPA}_J(q,\omega)\Big]_{J+1,J+1}\Big\}.$$

In the non-interacting case, $[\hat{\Pi}^{0}_J]_{pp'}$ being diagonal, (2.6) and (2.7) reduce to

$$R^0_T(q,\omega) = -\frac{1}{16\pi^2}\sum_{J=1}^{\infty}\Big\{(J+1)\,\mathrm{Im}\,\hat{\Pi}^0_{J-1}(q,\omega)+$$

$$+J\,\mathrm{Im}\,\hat{\Pi}^0_{J+1}(q,\omega)+(2J+1)\,\mathrm{Im}\,\hat{\Pi}^0_J(q,\omega)\Big\} \qquad (2.8)$$

and

$$R^0_L(q,\omega) = -\frac{1}{8\pi^2}\sum_{J=0}^{\infty}\Big\{J\,\mathrm{Im}\,\hat{\Pi}^0_{J-1}(q,\omega)+$$

$$+(J+1)\,\mathrm{Im}\,\hat{\Pi}^0_{J+1}(q,\omega)\Big\} \qquad (2.9)$$

It can be shown, with the help of (2.4), that the two expressions (2.8) and (2.9)in fact coincide.

The problem of calculating the nuclear spin-isospin responses is thus reduced to the one of solving the integral equation (2.3). We will pursue this task in the present paper, with the following parametrization of the spin-isospin particle-hole interaction [10]

$$\big[U_J(k)\big]_{\rho_1\rho_2} =$$

$$= a_{J\rho_1}a_{J\rho_2}V_L(k)+\big(\delta_{\rho_1\rho_2}-a_{J\rho_1}a_{J\rho_2}\big)V_T(k). \qquad (2.10)$$

In (2.10)

$$a_{J\rho} = (-1)^{\rho}\sqrt{2\rho+1}\begin{pmatrix}\rho & 1 & J\\ 0 & 0 & 0\end{pmatrix}, \qquad (2.11)$$

$$V_L(k) =$$

$$= \Gamma^2_\pi(k)\frac{f^2_\pi}{\mu^2_\pi}\left(\frac{g'}{k^2}-\frac{1}{k^2+\mu^2_\pi}\right) \qquad (2.12)$$

and

$$V_T(k) =$$

$$= \Gamma^2_\pi(k)\frac{f^2_\pi}{\mu^2_\pi}\frac{g'}{k^2}-\Gamma^2_\sigma(k)\frac{f^2_\sigma}{\mu^2_\sigma}\frac{1}{k^2+\mu^2_\sigma}. \qquad (2.13)$$

In these formulae g' is the Landau-Migdal parameter, $f^2_\pi/4\pi\hbar c = 0.08$, $f^2_\sigma/\mu^2_\sigma = 2.18(f^2_\pi/\mu^2_\pi)$ and $\Gamma_{\pi(\sigma)}(k)$ is the

usual dipole form factor of the $\pi(\varrho)$NN vertex (we shall use the cutoffs $\Lambda_\pi = 1.3$ GeV and $\Lambda_\varrho = 2.0$ GeV, respectively).

3. The solution of the RPA equations

If translational invariance holds, then $\hat{\Pi}^0_J(q,k;\omega)$ [being proportional to $\delta(q-k)$] picks out only one momentum in the integral of eq.(1.3), thus algebrizing the system of coupled integral equations. It is conceivable that for a nucleus large enough $\hat{\Pi}^0_J(q,k;\omega)$ will preserve a fairly diagonal behaviour, being peaked around $q=k$. If this is the case, then only a rather narrow band of momenta will effectively contribute to the integrals one faces when considering the subsequent iterations of eq.(2.3). This property is exploited in the method of Toki and Weise [11].

Indeed, according to them, it is possible to algebrize the whole problem, providing the "diagonal" behaviour of $\hat{\Pi}^0_J$ allows to invoke the mean value theorem in the first order iteration. More specifically one has to find an average momentum $\bar{q}$ such that

$$\int_0^\infty \frac{dk\,k^2}{(2\pi)^3} \sum_{\ell_1\ell_2} \left[\hat{\Pi}^0_J(q,k;\omega)\right]_{\ell\ell_1} \left[U_J(k)\right]_{\ell_1\ell_2} \left[\hat{\Pi}^0_J(k,q';\omega)\right]_{\ell_2\ell'} =$$

$$\simeq \gamma\,\frac{\bar{q}^2}{(2\pi)^3} \sum_{\ell_1\ell_2} \left[\hat{\Pi}^0_J(q,\bar{q};\omega)\right]_{\ell\ell_1} \left[U_J(\bar{q})\right]_{\ell_1\ell_2} \left[\hat{\Pi}^0_J(\bar{q},q';\omega)\right]_{\ell_2\ell'} \qquad (3.1)$$

$$\simeq \gamma\,\frac{\bar{q}^2}{(2\pi)^3} \sum_{\ell_1\ell_2} \left[\hat{\Pi}^0_J(\bar{q},\bar{q};\omega)\right]_{\ell\ell_1} \left[U_J(\bar{q})\right]_{\ell_1\ell_2} \left[\hat{\Pi}^0_J(q,q';\omega)\right]_{\ell_2\ell'}$$

where $\gamma \equiv \pi/R \simeq 0.9\ \mathrm{fm}^{-1}$ (R being the r.m.s. radius of the nucleus) roughly corresponds to the range of non-locality in momentum space.

While the first step in (3.1) directly follows from the mean value theorem, the subsequent one, which is the key point for the evaluation of the higher order iterations, is not trivial and will be shortly revisited in the Appendix A. There it is shown that the approximation (3.1) allows one to replace (2.3) with the matrix equation:

$$\left[\hat{\Pi}^{RPA}_J(q,q';\omega)\right]_{\ell\ell'} \cong \left[\hat{\Pi}^{\circ}_J(q,q';\omega)\right]_{\ell\ell'} +$$

$$+\frac{\gamma\,\bar{q}^2}{(2\pi)^3}\sum_{\ell_1\ell_2}\left[\hat{\Pi}^{\circ}_J(\bar{q},\bar{q};\omega)\right]_{\ell\ell_1}\left[U_J(\bar{q})\right]_{\ell_1\ell_2}\left[\hat{\Pi}^{RPA}_J(q,q';\omega)\right]_{\ell_2\ell'} \qquad (3.2)$$

As it stands (3.2) is, however, an oversimplification. *Indeed for fixed J five coupled (through the tensor interaction mediated by the pion and the rho) integral equations stem from (2.3): thus "a priori" one should introduce five average momenta* $\bar{q}_J(p,p')$. In this general case the expressions for the responses, obtained by solving (3.2) and by inserting the solutions in (2.6) and (2.7), turn out to be very cumbersome as it might be recognized in Appendix B, where they are reported. As a consequence the whole method becomes too complicated and no longer offers real advantages with respect to a straight numerical solution.

We have thus decided to disregard the differences, for a given J, among the various $\bar{q}_J(p,p')$. More precisely we fix the unique $\bar{q}_J$ directly on the first order approximation for the responses (2.6) and (2.7) thus avoiding the further problem connected with the actual existence of two $\bar{q}_J$,

arising from the real and imaginary part of (3.1).(*)

In this frame of work the two responses are given by the following expressions

$$R_T(q,\omega) = -\frac{1}{16\pi^2}\,\mathrm{Im}\sum_{J=1}^{\infty}\left\{\frac{(2J+1)\,\hat{\Pi}^{\circ}_J(q,\omega)}{1-\frac{\gamma\,\bar{q}^2}{(2\pi)^3}V_T(\bar{q})\,\hat{\Pi}^{\circ}_J(\bar{q},\omega)} + \right.$$

$$+\frac{(J+1)\,\hat{\Pi}^{\circ}_{J-1}(q,\omega)}{1-\frac{\gamma\,\bar{q}^2}{(2\pi)^3}V_T(\bar{q})\,\hat{\Pi}^{\circ}_{J-1}(\bar{q},\omega)+\frac{J}{2J+1}\mathcal{F}_{J+1}(\bar{q},\omega)} + \qquad (3.3)$$

$$\left.+\frac{J\,\hat{\Pi}^{\circ}_{J+1}(q,\omega)}{1-\frac{\gamma\,\bar{q}^2}{(2\pi)^3}V_T(\bar{q})\,\hat{\Pi}^{\circ}_{J+1}(\bar{q},\omega)+\frac{J+1}{2J+1}\mathcal{F}_{J-1}(\bar{q},\omega)}\right\}$$

with

$$\mathcal{F}_{J-1}(p,\omega) =$$

$$=\frac{\gamma\,p^2}{(2\pi)^3}\left[V_T(p)-V_L(p)\right]\frac{\hat{\Pi}^{\circ}_{J+1}(p,\omega)-\hat{\Pi}^{\circ}_{J-1}(p,\omega)}{1-\frac{\gamma\,p^2}{(2\pi)^3}V_L(p)\,\hat{\Pi}^{\circ}_{J-1}(p,\omega)} \qquad (3.4)$$

$$\mathcal{F}_{J+1}(p,\omega) =$$

$$=\frac{\gamma\,p^2}{(2\pi)^3}\left[V_T(p)-V_L(p)\right]\frac{\hat{\Pi}^{\circ}_{J-1}(p,\omega)-\hat{\Pi}^{\circ}_{J+1}(p,\omega)}{1-\frac{\gamma\,p^2}{(2\pi)^3}V_L(p)\,\hat{\Pi}^{\circ}_{J+1}(p,\omega)} \qquad (3.5)$$

and

(*) We notice that in the H.O. basis, which is utilized in the present paper, the exact first order $[\hat{\Pi}^{(\omega)}_J(q,q';\omega)]_{\ell\ell'}$ [left hand side of eq.(3.1)] can be analytically evaluated. This is done in Appendix C.

$$R_L(q,\omega) =$$

$$= -\frac{1}{8\pi^2}\,\mathrm{Im}\sum_{J=0}^{\infty}\left\{\frac{(J+1)\,\hat{\Pi}^{\circ}_{J+1}(q,\omega)}{1-\frac{\gamma\,\bar{q}^2}{(2\pi)^3}V_L(\bar{q})\,\hat{\Pi}^{\circ}_{J+1}(\bar{q},\omega)+\frac{J}{2J+1}\,\mathcal{G}_{J-1}(\bar{q},\omega)}+\right.$$

$$\left.+\frac{J\,\hat{\Pi}^{\circ}_{J-1}(q,\omega)}{1-\frac{\gamma\,\bar{q}^2}{(2\pi)^3}V_L(\bar{q})\,\hat{\Pi}^{\circ}_{J-1}(\bar{q},\omega)+\frac{J+1}{2J+1}\,\mathcal{G}_{J+1}(\bar{q},\omega)}\right\} \qquad (3.6)$$

with

$$\mathcal{G}_{J+1}(\bar{q},\omega) = \mathcal{F}_{J+1}(\bar{q},\omega\,;\,V_L\leftrightarrow V_T), \qquad (3.7)$$

$$\mathcal{G}_{J-1}(\bar{q},\omega) = \mathcal{F}_{J-1}(\bar{q},\omega\,;\,V_L\leftrightarrow V_T). \qquad (3.8)$$

In expresssions (3.3) and (3.6) a "nuclear matter like" partial wave expansion is recovered if the quantities $\mathcal{G}_J$ and $\mathcal{F}_J$ are omitted in the denominators. Their effect should therefore vanish in an infinite system. However, even when $\mathcal{G}_J$ and $\mathcal{F}_J$ are ignored, there remains a trace of the confinement of the system in the replacement $q\longrightarrow\bar{q}$ in the denominators.

The terms $\mathcal{G}_J$ and $\mathcal{F}_J$ embody the coupling discussed previously between the $\vec{\sigma}\times\vec{q}$ and $\vec{\sigma}\cdot\vec{q}$ spin modes as well as other contributions stemming from the gradient of the nuclear density. They can be sizable in the range of momenta where $q^2(V_T-V_L)$ is large, i.e. roughly for

$0.4\ \mathrm{fm}^{-1} \lesssim q \lesssim 2.1\ \mathrm{fm}^{-1}$ (see Fig.1).

The uncoupled responses are those obtained by letting the whole longitudinal $V_L(k)$ [respectively, transverse $V_T(k)$] interaction go to zero in (3.3) [(3.6)].

When this is done the following expressions are obtained

$$R_T^{\text{no-coupl}}(q,\omega) =$$

$$= -\frac{1}{16\pi^2}\,\mathrm{Im}\sum_{J=1}^{\infty}(2J+1)\left\{\frac{\hat{\Pi}^{\circ}_{J}(q,\omega)}{1-\frac{\gamma\,\bar{q}^2}{(2\pi)^3}V_T(\bar{q})\,\hat{\Pi}^{\circ}_{J}(\bar{q},\omega)}+\right. \qquad (3.9)$$

$$\left.+\frac{J\,\hat{\Pi}^{\circ}_{J+1}(q,\omega)+(J+1)\,\hat{\Pi}^{\circ}_{J-1}(q,\omega)}{(2J+1)-\frac{\gamma\,\bar{q}^2}{(2\pi)^3}V_T(\bar{q})\left[J\,\hat{\Pi}^{\circ}_{J+1}(\bar{q},\omega)+(2J+1)\,\hat{\Pi}^{\circ}_{J-1}(\bar{q},\omega)\right]}\right\}$$

and

$$R_L^{\text{no-coupl}}(q,\omega) =$$

$$= -\frac{1}{8\pi^2}\,\mathrm{Im}\sum_{J=0}^{\infty}(2J+1)\cdot \qquad (3.10)$$

$$\cdot\frac{(J+1)\,\hat{\Pi}^{\circ}_{J+1}(q,\omega)+J\,\hat{\Pi}^{\circ}_{J-1}(q,\omega)}{(2J+1)-\frac{\gamma\,\bar{q}^2}{(2\pi)^3}V_L(\bar{q})\left[(J+1)\,\hat{\Pi}^{\circ}_{J+1}(\bar{q},\omega)+J\,\hat{\Pi}^{\circ}_{J-1}(\bar{q},\omega)\right]}.$$

Before analyzing the results obtained, it is worthwhile to investigate the non-locality in momentum space of $\Pi^{\circ}_{\lambda\nu}(\vec{q},\vec{q}\,';\omega)$. Indeed, as shown in Appendix A, the TW approximation mostly relies on a well-peaked behaviour of Π° around $q=q'$.

In order to avoid the detailed analysis of the various multipoles, we focus our attention on the imaginary part of the density-density polarization propagator ($\mu = \nu = 0$, "time component").

At the same time we intend to explore how this quantity is affected by the size of the system. Thus we display in Fig.2 $\mathrm{Im}\,\Pi^{0}_{00}(\vec{q},\vec{q}';\omega)$ for fixed $q = 1.5\ \mathrm{fm}^{-1}$, $\hat{q}\cdot\hat{q}' = 1$ and $\hbar\omega \cong 55$ MeV as a function of q' for ^{16}O, ^{40}Ca and ^{80}Zr.

Notably the curves are bell shaped, showing a minimum for $q \cong q'$ in the case of the largest nucleus, whereas as the mass number decreases the minimum tends to be shifted at larger q'.

As expected, a substantial shrinking of the non-locality region is seen to occur as one moves from light to heavy nuclei. This outcome reflects the tendency toward the recovery of translational invariance, although a not-negligible amount of non-locality in momentum space (as well as in coordinate space) will always persist due to the very existence of the surface, no matter how large the nucleus.

Indeed the shrinking is more pronounced in going from ^{16}O to ^{40}Ca than from ^{40}Ca to ^{80}Zr. We can characterize the amount of non-locality by the half-height width $\Delta q'$ of the curves in Fig. 2: it turns out to be 1.2, 1.0 and 0.85 fm^{-1} for ^{16}O, ^{40}Ca and ^{80}Zr, respectively.

The ratios among these numbers closely follow the corresponding relationship among the surface to volume ratios (S/V) of the considered nuclei: their relative proportion is 1.36:1:0.79.

Non-locality in momentum space also depends upon the energy and tends to decrease as the energy becomes large. As a consequence we can expect that for a nucleus as large as ^{40}Ca the TW approximation is fairly reliable.

Moreover the new effects associated with the gradient of the nuclear density and the consequent mixing between $\vec{\sigma} \times \vec{q}$ and $\vec{\sigma}\cdot\vec{q}$ are likely to be more important at low energies, where non-locality is more appreciable. This will be illustrated in the next Section.

4. Results and discussion

We have performed the calculation in the case of ^{40}Ca, for which experimental data exist.

The resulting RPA transverse response is shown in Fig.3 at q = 330 MeV/c together with the corresponding nuclear matter response. An appreciable difference between the two shows up in the high energy region.

In order to explore the origin of this difference we have resorted to the semiclassical approach introduced by Schuck [5], which at least accounts for the confinement of the system.

It amounts to the following replacement

$$R_T = -\frac{4V}{\pi} \operatorname{Im} \Pi(q,\omega;k_F) \Rightarrow -16 \int_0^{R_c} dr\, r^2 \operatorname{Im} \Pi[q,\omega;k_F(r)], \qquad (4.1)$$

the local Fermi momentum being defined by the equation

$$\frac{\hbar^2 k_F^2(R)}{2m} + W(R) = \frac{\hbar^2 k_{F_0}^2}{2m} + W(0) \qquad (4.2)$$

The value of $k_F^2 \equiv k_F(0)$ is fixed by the condition

$$A = 4\pi \int_0^{R_c} dr\, r^2 \rho(r). \qquad (4.3)$$

For the potential well W(r) in (4.2) Schuck takes a realistic Wood-Saxon (WS)

$$W_{WS}(R) = \frac{V_0}{1+\exp\{(R-R_0)/a\}} \qquad (4.4)$$

with $V_0 = -50$ MeV, $R_0 = 1.2\ A^{1/3}$ fm and $a_0 = 0.5$ fm. In order to compare with our results we shall also consider an harmonic oscillator well (HO)

$$W_{HO}(R) = V_1 + \frac{1}{2} m \omega_0^2 R^2 \qquad (4.5)$$

with $V_1 = -55$ MeV and $\hbar\omega_0 = 41\ A^{-1/3}$ MeV.

This comparison will allow a test of the shortcomings stemming from the use of the Harmonic Oscillator model.

The upper limit of integration in (4.1) corresponds to the classical turning point for the single particle motion inside the nucleus and is set by the equation

$$k_F(R) = 0 \qquad (4.6)$$

which, e.g. for the Wood-Saxon well, yields

$$R_c = R_0 + a \ln\left[\frac{V_0}{V_0 + \hbar^2 k_{F_0}^2/2m} - 1\right] = 4.85 \text{ fm}. \qquad (4.7)$$

In Fig. 4 we display the semiclassical transverse response (4.1) for a WS and a HO well, compared with the nuclear matter RPA response. Discrepancies with the latter at high energies are present as well in the semiclassical approach.

The differences between HO and WS semiclassical results provide a feeling of the errors involved in the use of a HO basis with respect to a more realistic one. However this is the only basis which makes the present RPA calculation feasible.

We remark that the RPA renormalization is weaker for the HO semiclassical response than for the WS one; indeed the classical turning point for the HO ($R_c = 5.1$ fm) is larger than the WS one. The corresponding density is then smaller in the region between 2 and 4 fm, where the quantity $r^2 \rho(r)$ peaks. Thus less collectivity is present in the RPA HO response.

This feature, however, is not shared by our finite nucleus calculation, which is compared in Fig. 5 with the semiclassical approximation in the HO basis. Both our full RPA, expression (3.3), and the one where the gradient-density terms are omitted [equation (3.9)] are shown in the figure. The three curves are rather close at low energies, but our results display a more pronounced collectivity in the region of the maximum. Interestingly, the present calculation would approach the semiclassical one by using $\bar{q}_J = q$.

The differences between our two finite nucleus transverse responses is small (at most 10 %) showing the moderate influence in the volume response of the contribution stemming from the gradient density terms.

Notice that the coupling between $(\vec{\sigma}\cdot\vec{q})$ and $(\vec{\sigma}\times\vec{q})$ has practically no effect here, since at this particular momentum transfer the longitudinal force is relatively small (see also Table I). It should be remarked however that this is not a general feature valid for all q. Indeed, for example, at $q = 1.75$ fm^{-1} the influence of the $(\vec{\sigma}\cdot\vec{q})$

coupling in the transverse response may result in an increase up to 9-10%. Obviously the q-dependence of this effect has to be traced back to the one of V_L, which is rather pronounced owing to the small pionic mass.

On the contrary, as V_T is generally large, the transverse-longitudinal coupling sizeably affects the longitudinal response; this is displayed in Fig.6 where, together with the full finite nucleus calculation, the non-interacting response and the one without $(\vec{\sigma}\times\vec{q})$ mixing are shown (see also Table II).

These outcomes somehow disagree with previous investigations [12] of the role of the pion (respectively, of the rho-meson) in the transverse (longitudinal) channel.

Altogether the coupling between longitudinal and transverse, which occurs through the gradient density terms and which is the new feature of our approach is thus rather small in the global responses. However it plays a significant role when the separate multipoles of the responses are discussed.

Figs.7a,b show the renormalization factors $[R/R^0]_J$ of the transverse and longitudinal multipoles as a function of J. As expected the low multipoles which probe the nuclear interior are very collective and display a strong contrast between the longitudinal and transverse channels. On the other hand, collectivity is less pronounced for the higher multipolarities, which are peripheral and thus show less contrast even in the absence of the coupling.

The remarkable feature displayed in Figs.7a,b is that, in contrast to what happens for the low multipoles (and in

general for the volume responses), the coupling between $(\vec{\sigma}\cdot\vec{q})$ and $(\vec{\sigma}\times\vec{q})$ is extremely effective for the higher multipoles and produces a suppression of the contrast beyond what would be expected simply from the lowering of the density.

This suggests that the contrast is suppressed for peripheral probes such as (p,p') due to the coupling between the two channels at the nuclear surface. This may give the clue for the interpretation of the Los Alamos experiment [13], which has revealed no contrast. A detailed evaluation of the surface response requires a specific treatment and will be discussed in a forthcoming paper [9].

For the purpose of illustration we display in Fig.8 the ratio between the volume responses, R_L/R_T with and without the inclusion of the above discussed mixing and compare it with the same quantity calculated in nuclear matter.

A sizeable reduction of this ratio in the finite system is apparent. There remains however some contrast between the two responses, even when the transverse-longitudinal mixing is included. Therefore the present treatment, being limited to the volume responses, is not yet appropriate to account for the Los Alamos experiment which probes the nuclear surface.

A better testing ground for the present theory is the comparison with the transverse dynamic structure factor, as measured in (e,e') experiments. This quantity is linked to the polarization propagator and to our transverse response function (2.1) by the following definitions (m,n spherical indices)

$$S_T(\vec{q},\omega) = -\frac{\mu_o^2}{e^2}\left(\mu_p-\mu_n\right)^2 G_M^2(q_\lambda^2)\cdot$$

$$\cdot\frac{1}{\pi}\sum_{m,n}\left[J_{m,n}-(-1)^{m+n}\frac{1}{q^2}q_{-m}q_n\right]\mathrm{Im}\,\Pi_{m3,n3}(\vec{q},\vec{q};\omega)$$

$$=\frac{\mu_o^2}{e^2}\left(\mu_p-\mu_n\right)^2 G_M^2(q_\lambda^2)\,R_T(\vec{q},\omega) \qquad (4.8)$$

μ_o being the nuclear Bohr magneton, $\mu_p = 2.79$, $\mu_n = -1.91$ and

$$G_M(q_\lambda^2) = \frac{1}{\left[1+(\vec{q}^2-\omega^2/c^2)/(18.1\,fm^{-2})\right]^2} \qquad (4.9)$$

the usual electromagnetic γNN form factor. In (4.8) we have neglected the small isoscalar contribution.

We have calculated (4.8) for ^{40}Ca at q = 330, 370 and 410 MeV/c. Our results are reported in Figs.9, 10 and 11, where they are compared with the inclusive experiments of Saclay [1]. The dashed area in Fig.9 represents the "theoretical error" associated with the use of a HO basis rather than a WS one, deduced in the semiclassical approach as was illustrated in Fig.3.

First we note that the independent particle response does not reproduce the experimental data, as already remarked in ref.[10]. The RPA one, instead, when added to the 2p-2h contribution of ref.[3] gives a satisfactory agreement with the data.

The best agreement is obtained at 410 MeV/c, whereas at 330 MeV/c strength is clearly missing near the maximum of the response, whose position is, however, correctly reproduced. This outcome could reflect a q dependence of the Landau-Migdal parameter g', which could decrease at low momenta. The agreement at 410 MeV/c is suggestive of the persistence of a mild collective behaviour even at this momentum transfer.

The theoretical curves of Figs.9 to 11 show some extra strength, with respect to the experiment, on the low energy side. This failure does not appear in the semiclassical response which utilizes a WS potential. This can be seen in Fig.12 where the semiclassical transverse structure factor

$$S_T^{s.c.}(q,\omega) = -2\,\frac{\hbar^2 q^2}{m^2 c^2}\,(\mu_p-\mu_n)^2 \int_0^{R_c} dR\, R^2\, Im\,\Pi\left[q,\omega;k_F(R)\right] \qquad (4.10)$$

is displayed together with the full finite nucleus calculation. However (4.10) neglects the coupling between the spin modes as well as the gradient of the nuclear density which increase by a modest but (at low energy) significant amount the finite nucleus response.

The most likely explanation for the origin of this discrepancy is that our treatment of the 2p-2h excitations overestimates their importance at low energies, as it neglects RPA correlations in this sector.

In concluding this Section we note that with the present theory a reasonnable fit to the experimental data has been

obtained. The remaining discrepancies could be cured by the momentum dependence of g' and by a proper account for RPA correlations in the 2p-2h response.

Nevertheless we should not forget that we don't solve exactly, but only approximately, the RPA equations: although we believe that our results are good, we cannot claim that they are unaffected by some uncertainty. Indeed, beyond the algebrization of the exact integral equations, we have neglected here, as in the nuclear matter framework, the exchange matrix elements of the p-h force (although partially included in g'). However it may be worth pointing out that even our approcach would not have been reasonnably feasible without the use of a CRAY.

5. Conclusions

In this paper we have presented a RPA evaluation of the spin-isospin response function for a finite system. For this purpose we have utilized the approximation scheme suggested by Toki and Weise which allows analytical expressions for the responses themselves. This approach is particularly interesting since it admits a direct investigation of the new features introduced by the finite size of the system: namely the mixing between $(\vec{\sigma}\cdot\vec{q})$ and $(\vec{\sigma}\times\vec{q})$ couplings and the influence of the non-uniform density, which manifest themselves in terms involving the density gradient itself. These features have not been included in previous treatments.

We have given some arguments about the reliability of the TW approximation by analyzing the non-locality in momentum space of $\Pi^0(\vec{q},\vec{q}';\omega)$, which turns out to be sufficiently narrow to justify the approximation. For the same purpose we have compared the present theory with a semiclassical one, which embodies some of the effects associated with a non-uniform density, and we have found the corresponding responses to be rather close to each other. They both show some differences with respect to the nuclear matter response, particularly at high energy.

The semiclassical treatment also allows to get a feeling about the dependence of the theory upon the single particle basis, by comparing the semiclassical responses obtained with the HO and Wood Saxon potentials. Indeed some failures of

our finite nucleus calculation in the description of the experimental data would tend to be cured by the use of a more realistic WS basis.

Altogether the comparison of the present RPA theory (added to the 2p-2h contribution) with the transverse structure factor measured in (e,e') experiments is satisfactory. It eventually points out to a momentum dependence of g' (which should be lowered at small q).

We have given a particular attention to the mixing between the $(\vec{\sigma}\cdot\vec{q})$ and $(\vec{\sigma}\times\vec{q})$ couplings and to the gradient density terms, which are both ignored in the current treatments, namely the nuclear matter or semiclassical ones. Both of them tend to lower the collectivity of the RPA responses.

In the overall volume responses their effect remains small, of the order of 10% at most. The influence of the longitudinal coupling in the transverse response is q-dependent, reflecting the strong momentum dependence of the longitudinal p-h interaction.

The detailed analysis of the mixing between the two spin-couplings on the separate multipoles of the responses reveals interesting features: their influence is small for the low multipoles, which probe the nuclear interior. On the contrary the longitudinal-transverse mixing produces large modifications in the high multipoles, which are peripheral. Its effect tends to equalize the RPA renormalization of the longitudinal and transverse multipoles, thus suppressing the contrast between them.

Since these peripheral multipoles are the relevant ones in the surface responses [as the ones probed in (p, p') scattering] one can expect a severe reduction of the contrast between the longitudinal and transverse surface responses in spite of the existence of strong collective effects in the volume spin-isospin responses.

Appendix A

We shortly revisit here the hypothesis underlying the approximation method suggested by Toki and Weise [11]. Let us then consider the first order integral, eq. (3.1),

$$\hat{\Pi}^{(1)}_{J}(q,q';\omega) = \frac{1}{(2\pi)^3}\int_0^\infty dk\, k^2\, \hat{\Pi}^{0}_{J}(q,k;\omega)\, U_J(k)\, \hat{\Pi}^{0}_{J}(k,q';\omega) \qquad (A.1)$$

and assume that the non-local behaviour in momentum space of $\hat{\Pi}^{0}_{J}(q,q';\omega)$ can be reproduced as follows:

$$\hat{\Pi}^{0}_{J}(q,q';\omega) = g(q,\omega)\, d_J(q-q')\, g(q',\omega). \qquad (A.2)$$

In the above $g(q,\omega)$ is an appropriate function which we do not need specify, whereas $d_J(q-q')$ is a distribution function centered at the origin; it satisfies the following conditions:

$$d_J(0) = 1 \qquad (A.3)$$

$$\int_0^\infty dk\, d_J(q-k)\, d_J(k-q') = d_J(q-q') \qquad (A.4)$$

Formula (A.2) implies that $\hat{\Pi}^{0}_{J}(q,q';\omega)$ has a well defined maximum at $q = q'$, being fairly diagonal around it. If this is the case, then (A.1) becomes

$$\hat{\Pi}_J^{(4)}(q,q';\omega) =$$

$$= -\frac{1}{(2\pi)^3} g(q,\omega)\, g(q',\omega) \int_0^\infty dk\, k^2 g(k,\omega) U_J(k) g(k,\omega) \cdot \cdot d_J(q-k)\, d_J(k-q')$$

$$\simeq \frac{\gamma}{(2\pi)^3} \bar{q}^2 g(\bar{q},\omega)\, g(\bar{q},\omega) U_J(\bar{q}) \cdot \cdot g(q,\omega)\, g(q',\omega) \int_0^\infty dk\, d_J(q-k)\, d_J(k-q') \qquad (A.5)$$

where the mean value theorem has been utilized.

Using (A. 3) and (A. 4) it is now inmediate to get

$$\hat{\Pi}_J^{(1)}(q,q';\omega) \cong \frac{\gamma\, \bar{q}^2}{(2\pi)^3} \hat{\Pi}_J^{\circ}(\bar{q},\bar{q};\omega) U_J(\bar{q})\, \hat{\Pi}_J^{\circ}(q,q';\omega) \qquad (A.6)$$

which coincides with the last expression in (3. 1).

The same steps can now be performed in the subsequent iterations of the integral equation (2. 3); for the purpose of illustration let's consider the second order one:

$$\hat{\Pi}_J^{(2)}(q,q';\omega) = \frac{1}{(2\pi)^3} \int_0^\infty dk\, k^2\, \hat{\Pi}_J^{\circ}(q,k;\omega) U_J(k) \hat{\Pi}_J^{(1)}(k,q';\omega). \qquad (A.7)$$

With the help of (A. 6) one immediately gets

$$\hat{\Pi}_J^{(2)}(q,q';\omega) \simeq \frac{\gamma\, \bar{q}^2}{(2\pi)^3} \hat{\Pi}_J^{\circ}(\bar{q},\bar{q};\omega) U_J(\bar{q}) \cdot \cdot \int_0^\infty \frac{dk\, k^2}{(2\pi)^3} \hat{\Pi}_J^{\circ}(q,k;\omega) U_J(k) \hat{\Pi}_J^{\circ}(k,q';\omega)$$

$$\simeq \left[\frac{\gamma\, \bar{q}^2}{(2\pi)^3} \hat{\Pi}_J^{\circ}(\bar{q},\bar{q};\omega) U_J(\bar{q})\right]^2 \hat{\Pi}_J^{\circ}(q,q';\omega) \qquad (A.8)$$

thus the approximate algebraic form (3. 2) for the RPA equations is recovered.

There remains a subtle point in going from (A. 7) to (A. 8): indeed the $\bar{q}$ value introduced, in (A. 5), by the mean value theorem depends, in principle, upon q and q'. In the r. h. s. of (A. 7) one should use, therefore, a $\bar{q}(k,q')$ which in turn would inhibit the subsequent step. However the integrand of eq. (A. 5) depends upon q and q' through the product $d_J(q-k)\, d_J(k-q')$ which, owing to the well-peaked behaviour of the distribution function, will favour values of k within a relatively narrow band around $q \sim q'$. As a consequence $\bar{q}$ will be close to q (or q') and the first equality in (A. 8) appears to be justified.

Appendix B

Let us consider the five different contributions, at fixed J, to the first order polarization propagator: $[\hat{\Pi}^{(1)}_J]_{J-1,J-1}$, $[\hat{\Pi}^{(1)}_J]_{J+1,J+1}$, $[\hat{\Pi}^{(1)}_J]_{J,J}$, $[\hat{\Pi}^{(1)}_J]_{J-1,J+1}$ and $[\hat{\Pi}^{(1)}_J]_{J+1,J-1}$.

For each of them one finds, in principle, a different $\tilde{q}_J(1,1')$ which satisfies the approximate equality (3.1). Let us then use, as a short-hand notation: $p_1 \equiv \tilde{q}_J(J-1, J-1)$, $p_2 \equiv \tilde{q}_J(J+1, J-1)$, $p_3 \equiv \tilde{q}_J(J, J)$, $p_4 \equiv \tilde{q}_J(J-1, J+1)$, $p_5 \equiv \tilde{q}_J(J+1, J+1)$. Correspondingly the five (coupled) equations for $[\hat{\Pi}^{RPA}_J]_{gg'}$ will contain the various p_i, e.g.:

$$[\hat{\Pi}^{RPA}_J(q,q';\omega)]_{J-1,J-1} = \hat{\Pi}^{\circ}_{J-1}(q,q';\omega) + \\ + \frac{\gamma\, p_f^2}{(2\pi)^3}\Big\{\hat{\Pi}^{\circ}_{J-1}(p_1)\big[U_J(p_4)\big]_{J-1,J-1}\big[\hat{\Pi}^{RPA}_J(q,q';\omega)\big]_{J-1,J-1} + \\ + \hat{\Pi}^{\circ}_{J-1}(p_1)\big[U_J(p_3)\big]_{J-1,J+1}\big[\hat{\Pi}^{RPA}_J(q,q';\omega)\big]_{J+1,J-1}\Big\} \qquad (B.1)$$

$$\big[\hat{\Pi}^{RPA}_J(q,q';\omega)\big]_{J+1,J-1} = \\ = \frac{\gamma\, p_f^2}{(2\pi)^3}\Big\{\hat{\Pi}^{\circ}_{J+1}(p_2)\big[U_J(p_3)\big]_{J+1,J-1}\big[\hat{\Pi}^{RPA}_J(q,q';\omega)\big]_{J-1,J-1} + \\ + \hat{\Pi}^{\circ}_{J+1}(p_2)\big[U_J(p_5)\big]_{J+1,J+1}\big[\hat{\Pi}^{RPA}_J(q,q';\omega)\big]_{J+1,J-1}\Big\} \qquad (B.2)$$

With a tedious but straigthforward calculation one can solve them and insert the expressions for the different RPA multipoles into (2.6) and (2.7). The resulting transverse and longitudinal response functions read:

$$R_T(q,\omega) = -\frac{1}{16\pi^2}\,\mathrm{Im}\sum_{J=1}^{\infty}\Big\{\frac{(2J+1)\,\hat{\Pi}^{\circ}_J(q,q;\omega)}{1-\vartheta_T(p_3)\,\hat{\Pi}^{\circ}_J(p_3,\omega)} + \\ + \frac{(J+1)\,\hat{\Pi}^{\circ}_{J-1}(q,q;\omega)}{1-\vartheta_T(p_1)\,\hat{\Pi}^{\circ}_{J-1}(p_1,\omega)+\mathcal{C}_{J-1}(p_1,p_2)} + \\ + \frac{J\,\hat{\Pi}^{\circ}_{J+1}(q,q;\omega)}{1-\vartheta_T(p_4)\,\hat{\Pi}^{\circ}_{J+1}(p_4,\omega)+\mathcal{C}_{J+1}(p_4,p_5)}\Big\} \qquad (B.3)$$

where

$$\mathcal{C}_{J-1}(p,p') = \frac{J}{2J+1}\Big\{\hat{\Pi}^{\circ}_{J-1}(p,\omega)\big[\vartheta_T(p)-\vartheta_L(p)\big] - \\ - \hat{\Pi}^{\circ}_{J+1}(p',\omega)\big[\vartheta_T(p')-\vartheta_L(p')\big]\,\frac{1-\vartheta_L(p)\,\hat{\Pi}^{\circ}_{J-1}(p,\omega)}{1-\vartheta_L(p')\,\hat{\Pi}^{\circ}_{J+1}(p',\omega)}\Big\} \qquad (B.4)$$

$$\mathcal{C}_{J+1}(p,p') = \frac{J+1}{2J+1}\Big\{\hat{\Pi}^{\circ}_{J+1}(p,\omega)\big[\vartheta_T(p)-\vartheta_L(p)\big] - \\ - \hat{\Pi}^{\circ}_{J-1}(p',\omega)\big[\vartheta_T(p')-\vartheta_L(p')\big]\,\frac{1-\vartheta_L(p)\,\hat{\Pi}^{\circ}_{J+1}(p,\omega)}{1-\vartheta_L(p')\,\hat{\Pi}^{\circ}_{J-1}(p',\omega)}\Big\} \qquad (B.5)$$

and

$$R_L(q,\omega) =$$

$$= -\frac{1}{8\pi^2}\,\mathrm{Im}\sum_{J=0}^{\infty}\left\{\frac{J\,\hat{\Pi}^{\circ}_{J-1}(q,q;\omega)}{1-\vartheta_L(p_1)\hat{\Pi}^{\circ}_{J-1}(p_1,\omega)+\mathcal{L}_{J-1}(p_1,p_2)}+\right.$$

$$\left.+\frac{(J+1)\,\hat{\Pi}^{\circ}_{J+1}(q,q;\omega)}{1-\vartheta_L(p_4)\hat{\Pi}^{\circ}_{J+1}(p_4,\omega)+\mathcal{L}_{J+1}(p_4,p_5)}\right\} \qquad (B.6)$$

where

$$\mathcal{L}_{J-1}(p,p') = \frac{J+1}{J}\,\mathcal{C}_{J-1}\{p,p';\vartheta_L\leftrightarrow\vartheta_T\} \qquad (B.7)$$

$$\mathcal{L}_{J+1}(p,p') = \frac{J}{J+1}\,\mathcal{C}_{J+1}\{p,p';\vartheta_L\leftrightarrow\vartheta_T\} \qquad (B.8)$$

In the above formulas

$$\vartheta_L(p) = \gamma\,\frac{p^2}{(2\pi)^3}V_L(p) \qquad (B.9)$$

$$\vartheta_T(p) = \gamma\,\frac{p^2}{(2\pi)^3}V_T(p) \qquad (B.10)$$

One can easily show that when all the p_i coincide the expressions (1.3) to (1.8) are recovered.

Appendix C

We derive here, using an Harmonic Oscillator basis and the interaction (2.10) the exact analytic expression for the first order polarization propagator $\{\hat{\Pi}^{(1)}_J\}_{\ell\ell'}$. In particular we consider its imaginary part, which is the one actually used for the determination of $\bar{\alpha}_J$. It reads:

$$\mathrm{Im}\left[\hat{\Pi}^{(1)}_J(q,q';\omega)\right]_{\ell\ell'} \equiv$$

$$\equiv \frac{1}{(2\pi)^3}\int_0^{\infty} dk\,k^2\left[U_J(k)\right]_{\ell\ell'}\left\{\mathrm{Im}\,\hat{\Pi}^{\circ}_{\ell}(q,k;\omega)\,\mathrm{Re}\,\hat{\Pi}^{\circ}_{\ell'}(k,q';\omega)+\right.$$

$$\left.+\mathrm{Re}\,\hat{\Pi}^{\circ}_{\ell}(q,k;\omega)\,\mathrm{Im}\,\hat{\Pi}^{\circ}_{\ell'}(k,q';\omega)\right\}, \qquad (C.1)$$

which, by defining

$$\Delta_{ph} = -\pi\,\delta\left[\hbar\omega-\left(\epsilon_{n_p\ell_p}-\epsilon_{n_k\ell_k}\right)\right]$$

$$= -\frac{\pi}{\hbar\omega_o}\,\delta\left(\Delta N - N_p + N_k\right) \qquad (C.2)$$

and

$$E_{ph} = \begin{cases} -\dfrac{1}{2\hbar\omega}, & \text{if } \hbar\omega = \epsilon_{n_p\ell_p}-\epsilon_{n_k\ell_k} \\ \dfrac{2\left(\epsilon_{n_p\ell_p}-\epsilon_{n_k\ell_k}\right)}{(\hbar\omega)^2-\left(\epsilon_{n_p\ell_p}-\epsilon_{n_k\ell_k}\right)^2}, & \text{if } \hbar\omega \neq \epsilon_{n_p\ell_p}-\epsilon_{n_k\ell_k} \end{cases} \qquad (C.3)$$

where $N_{p,h} = 2n_{p,h} + \ell_{p,h} + 3/2$ and $\hbar\omega_0$ is the harmonic oscillator parameter, can be recast in the following form

$$\mathrm{Im}\left[\hat{\Pi}^{(4)}_J(q,q';\omega)\right]_{\ell\ell'} =$$

$$= \frac{32}{\pi} \sum_{\substack{n_p \ell_p \\ n_h \ell_h}} \sum_{\substack{n'_p \ell'_p \\ n'_h \ell'_h}} (2\ell_p+1)(2\ell_h+1)(2\ell'_p+1)(2\ell'_h+1) \begin{pmatrix} \ell_p & \ell_h & \ell \\ 0 & 0 & 0 \end{pmatrix}^2 \begin{pmatrix} \ell'_p & \ell'_h & \ell' \\ 0 & 0 & 0 \end{pmatrix}^2 \cdot$$

$$\cdot \mathcal{J}_{\ell n_p \ell_p n_h \ell_h}(q)\, \mathcal{J}_{\ell' n'_p \ell'_p n'_h \ell'_h}(q') \left[\Delta_{ph} E_{p'h'} + E_{ph} \Delta_{p'h'}\right] \cdot \qquad (C.4)$$

$$\cdot \int_0^\infty dk\, k^2 \left[U_J(k)\right]_{\ell\ell'} \mathcal{J}_{\ell n_p \ell_p n_h \ell_h}(k)\, \mathcal{J}_{\ell' n'_p \ell'_p n'_h \ell'_h}(k).$$

The above integral, recalling the analytic expression for $\mathcal{J}_{\ell n_p \ell_p n_h \ell_h}(k)$ given in the Appendix of ref.[10] and neglecting the k-dependence of the $\pi(\varrho)NN$ vertex form factor, turns out to be of the type

$$I(2n) = \int_0^\infty dk\, e^{-k^2/2\nu} \frac{1}{k^2 + b^2} k^{2n} \qquad (C.5)$$

b ($= \mu_\pi$ or μ_ς) being a constant, n an integer ≥ 1, $\nu = m\omega_0/\hbar$ and can be analytically evaluated by utilizing the following, easily established, recursion relation

$$I(2n) = \sqrt{\frac{\pi\nu}{2}}\, \nu^{n-1} (2n-3)!! - b^2 I(2n-2) \qquad (C.6)$$

together with the well-known formula [14]

$$I(0) = \frac{\pi}{2b} e^{b^2/2\nu} \operatorname{erfc}\left(\frac{b}{\sqrt{2\nu}}\right). \qquad (C.7)$$

The definition

$$\operatorname{erfc}(x) = \frac{2}{\sqrt{\pi}} \int_x^\infty e^{-t^2} dt \qquad (C.8)$$

has been used for the error function.

The final result reads

$$\mathrm{Im}\left[\hat{\Pi}^{(4)}_J(q,q';\omega)\right]_{\ell\ell'} =$$

$$= \frac{32\,\nu}{2^{(\ell+\ell')/2}\pi} \sqrt{\frac{\pi\nu}{2}} \sum_{\substack{n_p \ell_p \\ n_h \ell_h}} \sum_{\substack{n'_p \ell'_p \\ n'_h \ell'_h}} (2\ell_p+1)(2\ell_h+1)(2\ell'_p+1)(2\ell'_h+1) \cdot$$

$$\cdot \begin{pmatrix} \ell_p & \ell_h & \ell \\ 0 & 0 & 0 \end{pmatrix}^2 \begin{pmatrix} \ell'_p & \ell'_h & \ell' \\ 0 & 0 & 0 \end{pmatrix}^2 \mathcal{J}_{\ell n_p \ell_p n_h \ell_h}(q)\, \mathcal{J}_{\ell' n'_p \ell'_p n'_h \ell'_h}(q') \cdot$$

$$\cdot \left[\Delta_{ph} E_{p'h'} + E_{ph} \Delta_{p'h'}\right] \cdot \qquad (C.9)$$

$$\cdot \left[\frac{s_f(p_p,n_p)\, s_f(p_h,n_h)}{2^{n_p+n_h}\, n_p!\, n_h!} \cdot \frac{s_f(p'_p,n'_p)\, s_f(p'_h,n'_h)}{2^{n'_p+n'_h}\, n'_p!\, n'_h!}\right]^{1/2} \cdot$$

$$\cdot \sum_{k=0}^{n_p} \sum_{k'=0}^{n_h} \sum_{n=0}^{n'_p} \sum_{n'=0}^{n'_h} \binom{n_p}{k} \binom{n_h}{k'} \binom{n'_p}{n} \binom{n'_h}{n'} \frac{(-1)^{k+k'+n+n'}\, s_f(p,M)\, s_f(p',M')}{s_f(p_p,k)\, s_f(p_h,k')\, s_f(p'_p,n)\, s_f(p'_h,n')} \cdot$$

$$\cdot \sum_{m=0}^{M} \sum_{m'=0}^{M'} \left(-\frac{1}{2}\right)^{m+m'} \binom{M}{m} \binom{M'}{m'} \frac{1}{s_f(p,m)\, s_f(p',m')} \left[V_J(N)\right]_{\ell\ell'}$$

where

$$[V_T(N)]_{\ell\ell'} = \alpha_\pi\, g'\, \delta_{\ell\ell'}\,(2N-1)!! +$$

$$+ \alpha_\sigma\left(\alpha_{T\ell}\,\alpha_{T\ell'} - \delta_{\ell\ell'}\right)\left[\sum_{s=0}^{N}(-1)^s\left(\frac{\mu_\sigma^2}{\nu}\right)^s(2N-2s-1)!! + \right.$$

$$\left. + \left(-\frac{\mu_\sigma^2}{\nu}\right)^{N+1}\sqrt{\frac{\pi\nu}{2\mu_\sigma^2}}\, e^{\mu_\sigma^2/2\nu}\, erfc\left(\frac{\mu_\sigma}{\sqrt{2\nu}}\right)\right] -$$

$$- \alpha_\pi\,\alpha_{T\ell}\,\alpha_{T\ell'}\left[\sum_{s=0}^{N}(-1)^s\left(\frac{\mu_\pi^2}{\nu}\right)^s(2N-2s-1)!! + \right. \qquad \text{(C.10)}$$

and the definitions

$$\left. + \left(-\frac{\mu_\pi^2}{\nu}\right)^{N+1}\sqrt{\frac{\pi\nu}{2\mu_\pi^2}}\, e^{\mu_\pi^2/2\nu}\, erfc\left(\frac{\mu_\pi}{\sqrt{2\nu}}\right)\right]$$

$$sf(\ell,n) = (2\ell+2n+1)!! \qquad \text{(C.11)}$$

$$N = m+m'+1+(\ell+\ell')/2 \qquad \text{(C.12a)}$$

$$M = (\ell_p+\ell_h-\ell)/2 + K + K' \qquad \text{(C.12b)}$$

$$M' = (\ell_p'+\ell_h'-\ell')/2 + n + n' \qquad \text{(C.12c)}$$

$$\alpha_\pi = \Gamma_\pi^2(q^2)\,\frac{\beta_\pi^2}{\mu_\pi^2} \qquad \text{(C.12d)}$$

$$\alpha_\sigma = \Gamma_\sigma^2(q^2)\,\frac{\beta_\sigma^2}{\mu_\sigma^2} \qquad \text{(C.12e)}$$

have been used.

References

(1) Z.S.Meziani et al., Phys.Rev.Lett. 54 (1985) 1233

(2) W.M.Alberico, M.Ericson and A.Molinari, Nucl.Phys. A379 (1982) 429

(3) W.M.Alberico, M.Ericson and A.Molinari, Ann. of Phys. (N.Y.) 154 (1984) 356

(4) H.Esbensen and G.F.Bertsch, Ann. of Phys. 157 (1984) 255

(5) P.Schuck, Lecture Notes on the Random Phase Approximation (Trieste, february 1984):
U.Stroth, R.W.Hasse, P.Schuck, Proc. Intern. Symp. on Highly Excited States and Nuclear Structure (Orsay, 1983)

(6) M. Cavinato, D. Drechsel, E. Fein, M. Marangoni and A. M. Saruis, Nucl. Phys. A423 (1984) 376

(7) U.Stroth, R.W.Hasse, P.Schuck, W.M.Alberico, A.Molinari and M.Ericson, Phys.Lett. 156B (1985) 291

(8) J.Delorme, M.Ericson, A.Figureau and C.Thevenet, Ann. of Phys. 102 (1976) 273

(9) W.M.Alberico, A.De Pace, M.Ericson, M.B.Johnson and A.Molinari, in preparation

(10) W.M.Alberico, A.De Pace and A.Molinari, Phys.Rev. C31 (1985) 2007

(11) H.Toki and W.Weise, Phys.Rev.Lett. 42 (1979) 1034
H.Toki and W.Weise, Z.Physik A292 (1979) 389

(12) J.Cohen, Phys.Rev. C30 (1984) 1573

(13) T.A.Carey et al., Phys.Rev.Lett. 53 (1984) 144

(14) M.Abramowitz and I.Stegun, Handbook of mathematical functions, Dover Publ.Inc. (N.Y., 1972) p.297

Table Captions

Table I

Detailed transverse responses for ^{40}Ca at q= 330 MeV/c. Column 3 contains the independent particle response, column 4 the full RPA calculation, column 5 ($R_T^{RPA}(1)$) the one without mixing of $V_L(q)$ and column 6 ($R_T^{RPA}(2)$) the transverse response without influence of the gradient density terms. The responses are in $(MeV*fm^2)^{-1}$. P_1 and P_2 are defined as follows

$$P_1 = \frac{R_T^{RPA} - R_T^{RPA}(1)}{R_T^{RPA}}$$

$$P_2 = \frac{R_T^{RPA} - R_T^{RPA}(2)}{R_T^{RPA}}$$

Table II

The same as Table I for the longitudinal responses.

Figure Captions

Figure 1 - The difference between the transverse and longitudinal interactions multiplied by $[q^2/(2\pi)^3]$ as a function of q.

Figure 2 - The imaginary part of $\Pi^0_{p,h}(\vec{q},\vec{q}';\omega)/A$ at fixed $q = 1.5$ fm^{-1}, $\hbar\omega \cong 55$ MeV and $\hat{q}\cdot\hat{q}' = 1$, as a function of q' for ^{16}O (dashed line), ^{40}Ca (dot-dashed line) and ^{80}Zr (continuous line). The energy is only approximately the same in the three curves since each nucleus keeps its own HO parameter (55 MeV roughly correspond to $4\hbar\omega_0$ in ^{16}O, $5\hbar\omega_0$ in ^{40}Ca and $6\hbar\omega_0$ in ^{80}Zr).

Figure 3 - Free and RPA transverse responses for ^{40}Ca at $q = 330$ MeV/c as a function of $\hbar\omega$. The continuous and the dotted lines correspond to the finite nucleus calculation, the dot-dashed and the dashed lines correspond to the infinite nuclear matter responses with a Fermi momentum $k_F = 1.2$ fm^{-1}.

Figure 4 - Free and RPA semiclassical transverse responses for ^{40}Ca at $q = 330$ MeV/c as a function of $\hbar\omega$. The dotted and dash-dotted lines refer to the HO potential; the dashed and continuous lines refer to the WS one. The infinite nuclear matter RPA response (double dot-dashed line) is the same as in Fig. 3.

Figure 5 - RPA transverse responses for ^{40}Ca at $q = 330$ MeV/c as a function of $\hbar\omega$. The dot-dashed line is the semiclassical response with the HO potential; the continuous line is the full RPA finite nucleus calculation and the dashed line the one where the gradient density terms are omitted.

Figure 6 - The longitudinal responses of ^{40}Ca at $q = 330$ MeV/c as a function of $\hbar\omega$. The dot-dashed line is the independent particle response, the continuous line the full RPA finite nucleus calculation and the dashed line the one where the mixing of $V_T(q)$ is omitted.

Figure 7 - (a) Ratios of RPA and independent particle multipoles contributing to the finite nucleus responses, at fixed $q = 330$ MeV/c and $\hbar\omega = 1\ \hbar\omega_0$ as a function of J. The dashed lines refer to the calculation without $(\vec{\sigma}\cdot\vec{q})$ [respectively $(\vec{\sigma}\times\vec{q})$] mixing in the transverse [longitudinal] channel. The continuous lines refer to the full RPA calculation. Upper and lower curves represent the longitudinal and transverse channels, respectively.
(b) the same as in (a) but at $\hbar\omega = 2\ \hbar\omega_0$.

Figure 8 - The ratio between the RPA longitudinal and transverse responses for ^{40}Ca at $q = 1.75$ fm^{-1} as a function of $\hbar\omega_0$. The continuous line refers to the full RPA calculation, the dashed line to the one where the gradient density terms are omitted. The dot-dashed line is the ratio between the infinite nuclear matter responses with $k_F = 1.2$ fm^{-1}.

Figure 9 - The transverse dynamic structure factor of ^{40}Ca measured in (e,e') inelastic scattering as a function of $\hbar\omega$, at fixed momentum transfer q = 330 MeV/c. The experimental points are taken from ref. 1. The dot-dashed line refers to the independent particle response, the dashed line to the present RPA calculation and the continuous line is obtained by adding to the latter the 2p-2h contribution (double dot-dashed line) of ref. 3.

Figure 10 - The same as Fig. 9, at q = 370 MeV/c.

Figure 11 - The same as Fig. 9, at q = 410 MeV/c.

Figure 12 - The transverse dynamic structure factor of ^{40}Ca measured in (e,e') inelastic scattering as a function of $\hbar\omega$, at fixed momentum transfer q = 330 MeV/c. The experimental points are taken from ref. 1. The theoretical curves are obtained in the semiclassical approach with a WS potential. The dot-dashed line is the free response, the dashed line the RPA one and the continuous line is the sum of the latter with the 2p-2h contribution of ref. 3. For comparison the finite nucleus total response of Fig. 9 is also displayed (double dot- dashed line).

Table I

$\hbar\omega$ (MeV)	$\frac{\hbar\omega}{\hbar\omega_0}$	R_T^0	R_T^{RPA}	$R_T^{RPA}(1)$	$R_T^{RPA}(2)$	P_1	P_2
11.02	1	0.194	0.072	0.070	0.065	2.62%	9.66%
22.04	2	0.377	0.141	0.138	0.131	2.06%	7.28%
33.06	3	0.499	0.192	0.188	0.179	1.89%	6.87%
44.08	4	0.550	0.234	0.229	0.220	1.85%	6.02%
55.10	5	0.572	0.265	0.261	0.251	1.62%	5.48%
66.12	6	0.566	0.282	0.279	0.269	1.24%	4.66%
77.14	7	0.524	0.284	0.279	0.272	1.00%	4.33%
88.16	8	0.442	0.277	0.275	0.267	0.61%	1.61%
99.18	9	0.335	0.251	0.250	0.244	0.12%	2.63%

Table II

$\hbar\omega$ (MeV)	$\frac{\hbar\omega}{\hbar\omega_0}$	R_L^0	R_L^{RPA}	$R_L^{RPA}(1)$	$R_L^{RPA}(2)$	P_1	P_2
11.02	1	0.194	0.266	0.286	0.287	7.72%	8.17%
22.04	2	0.377	0.502	0.533	0.550	6.16%	9.53%
33.06	3	0.499	0.592	0.628	0.628	6.18%	6.10%
44.08	4	0.550	0.618	0.647	0.643	4.71%	4.14%
55.10	5	0.572	0.607	0.628	0.624	3.46%	2.81%
66.12	6	0.566	0.566	0.583	0.574	3.15%	1.50%
77.14	7	0.524	0.512	0.520	0.515	1.66%	0.70%
88.16	8	0.442	0.417	0.424	0.416	1.53%	-0.24%
99.18	9	0.335	0.323	0.324	0.322	0.31%	-0.28%

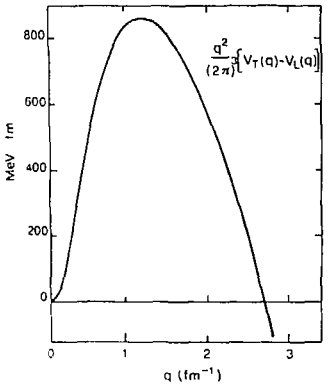

Figure 1

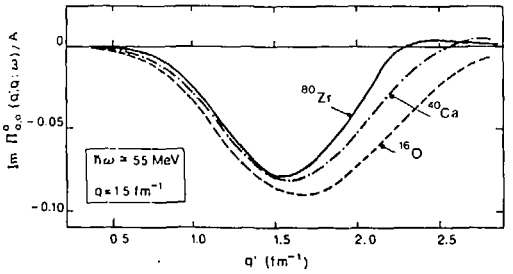

Figure 2

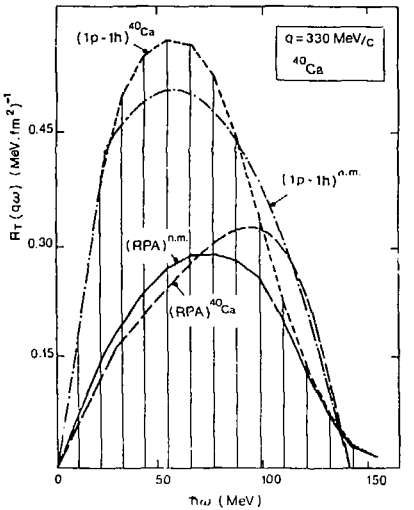

Figure 3

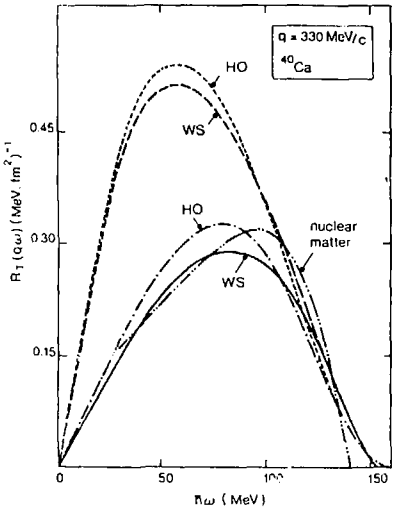

Figure 4

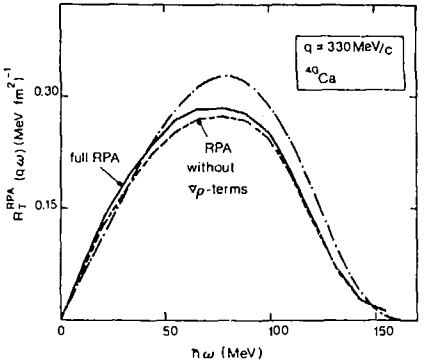

Figure 5

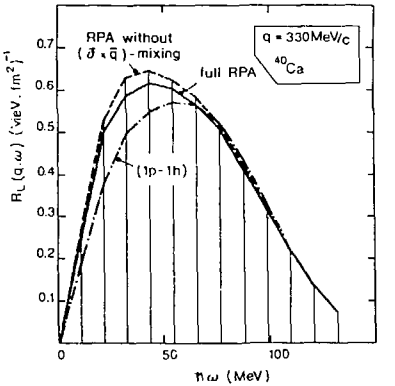

Figure 6

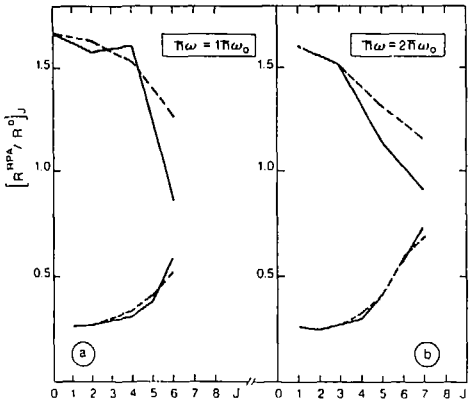

Figure 7

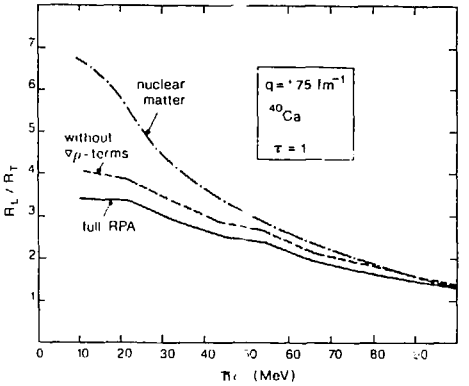

Figure 8

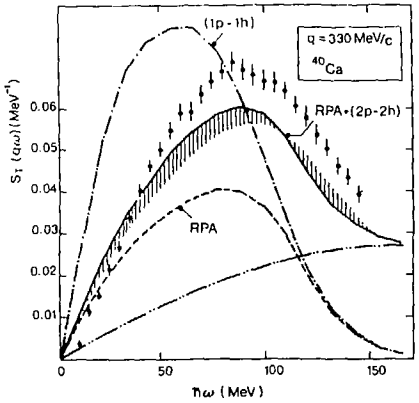

Figure 9

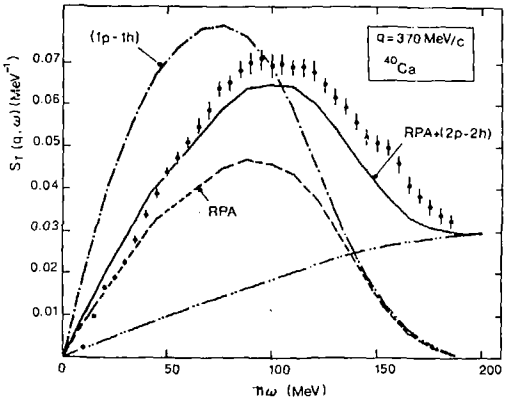

Figure 10

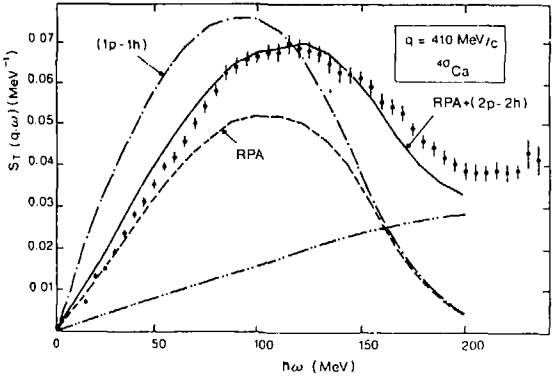

Figure 11

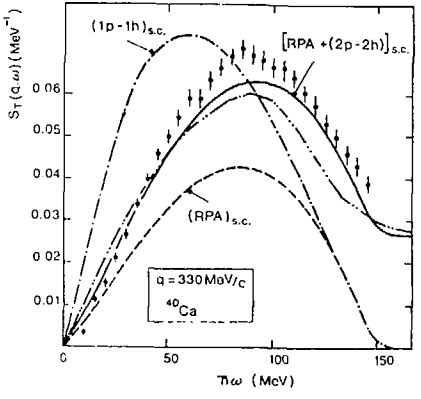

Figure 12